Science Arts & Métiers (SAM)
is an open access repository that collects the work of Arts et Métiers Institute of Technology researchers and makes it freely available over the web where possible.

This is an author-deposited version published in: https://sam.ensam.eu
Handle ID: .http://hdl.handle.net/10985/17951

To cite this version :

Taoufik QORIA, François GRUSON, Frédéric COLAS, Guillaume DENIS, Thibault PREVOST, Xavier GUILLAUD - Critical clearing time determination and enhancement of grid-forming converters embedding virtual impedance as current limitation algorithm - IEEE Journal of Emerging and Selected Topics in Power Electronics p.11 - 2019

Any correspondence concerning this service should be sent to the repository Administrator : archiveouverte@ensam.eu

Critical clearing time determination and enhancement of grid-forming converters embedding virtual impedance as current limitation algorithm

Taoufik Qoria, François Gruson, *Member, IEEE*, Fréderic Colas, *Member, IEEE*, Guillaume Denis, Thibault Prevost, Xavier Guillaud, *Member, IEEE,*

***Abstract*— The present paper deals with the post-fault synchronization of a voltage source converter based on the droop control. In case of large disturbances on the grid, the current is limited via current limitation algorithms such as the virtual impedance. During the fault, the power converter internal frequency deviates resulting in a converter angle divergence. Thereby, the system may lose the synchronism after fault clearing and which may lead to instability. Hence, this paper proposes a theoretical approach to explain the dynamic behavior of the grid forming converter subject to a three phase bolted fault. A literal expression of the critical clearing time is defined. Due to the precise analysis of the phenomenon, a simple algorithm can be derived to enhance the transient stability. It is based on adaptive gain included in the droop control. These objectives have been achieved with no external information and without switching from one control to the other. To prove the effectiveness of the developed control, experimental test cases have been performed in different faulted conditions.**

***Index Terms*— Grid forming voltage source converter, virtual impedance, current limitation, droop control, transient stability.**

I. Introduction

Grid-forming Voltage Source Converter (VSC) based on the droop control [1] has been widely studied in Microgrid and uninterruptible power supply for several types of applications: stability analysis in islanding mode [2], active and reactive power sharing in parallel operation [3], [4], decoupling control of active and reactive power [5]). These studies have been recently extended to power transmission systems dominated by renewable energy sources [6] where new challenges appear such as power converter controllers tuning for stable operation in case of low switching frequency [7], [8], stability assessment for large power system [6], optimal placement of grid-forming converters in large power system [9].

Unlike grid-following converters that behave as current sources, grid-forming converters are very sensitive to external disturbances. Indeed, due to the voltage source behavior of a grid forming converter, the overcurrent protection deserves a specific attention [10]–[12]. Compared to synchronous generators (SGs) that can support up to seven times over their rated current, power converters can only cope with few percent of overcurrent 20% to 40%. Trying to mimic synchronous machine would require a very large oversizing of semiconductor components and induces large additional costs. Therefore, power converters have to be protected against extreme events as short circuits but also other events which may induce small overcurrent: phase shift, connection of large loads and tripping of a line [13].

Many control strategies have been proposed for grid-forming converter in order to limit the current during transients. One strategy is to limit the current with a saturated control algorithm. This control strategy has been implemented in different ways e.g.; [11], [14], [15]. Despite that the current saturation limits the current during transient; if no PLL is implemented, the voltage controller will not be able to keep the output AC voltage aligned with the grid one. Thereby, the system can become unstable during the post-fault phase [12].

Recently, innovative concepts based on Virtual Impedance (VI) [10], [12], [16]–[18] have been implemented to emulate the effect of a physical impedance when the current exceeds its nominal value. These methods have shown their effectiveness to limit the current transients in case of lines tripping [10] and heavy load connection [12] while keeping the same nature of the power source “i.e.; voltage source”. Moreover, they ensure more stability in comparison to the current saturation [12]. Hence, the virtual impedance control proposed in [12], [17] is adopted in this paper.

Conventionally, if a power converter loses the synchronism and becomes unstable after large disturbances, it will be disconnected from the main grid for safety purposes [19]. However, in future power systems dominated by renewable energy sources (RESs), grid-forming converters have not only to cope with current limitation, but also to feed loads and provide services to the main grid even after fault clearing. In the literature, some papers proposed to switch from voltage

control based on the droop control to the PLL-based current control [1], [20] in order to maintain the synchronism and to ensure a transient stability. These methods require a complex algorithm for fault detection, triggering conditions. Moreover, as specified by [1], fault recovery could only be achieved after a considerable retuning of the voltage controller and the power controller in order to avoid AC voltage collapse. Recently, the transient stability mechanism of the current source VSC based on the droop control has been discussed in the literature in [14], [21]–[23] in case of operating point change and a 50% voltage sag. However, to the best of our knowledge, the post-fault synchronization of the VSC based on droop control and virtual impedance operating as voltage source has not been discussed in the literature. Hence, the contributions of the present paper consist to:

- Explain theoretically the synchronization process of a VSC based on droop control and virtual impedance when it is subjected to large disturbances such as a three-phase bolted fault.
- Propose an adaptive droop control to increase the critical clearing time and to limit the angle variation during the fault, and thereby, to enhance the system dynamics and its transient stability after fault clearing.

This paper is mainly focused on a grid forming control with a negligible inertial effect, which allows to develop some simplified analytical expressions and to give some general considerations in term of transient stability analysis. Since the inertial effect can be modified by the control, it is also interesting to study the case when it is not negligible. Simplified approaches are not possible anymore, however, it is still possible to use the same methodology, thanks to the simulation results, to evaluate the transient stability and enhance the critical clearing time.

Contrary to the conventional methods where the control has to switch from one strategy to another one (e.g.; from droop control to PLL), or require a triggering condition to avoid a transient instability after fault clearing, the proposed control does not need to switch to other strategies during fault which simplifies its analysis.

To show the effectiveness of the developed control in ensuring a current limitation as well as stable post fault synchronization, an experimental test bench has been developed to validate the proposed control algorithm.

The reminder of this paper is organized as follow. Section II first describes the studied system and its control structure, then, it recalls the operation principle of the virtual impedance for current limitation and shows its impact on the system dynamics. Section III presents the synchronization process of the grid-forming based droop control during and after fault clearing. Section IV proposes a variable droop control to enhance the transient stability of the power converter. Section V presents the developed experimental bench and the experimental validation of the proposed control.

II. Grid-Forming Voltage Source Converter Based on Droop Control and Virtual Impedance

A. Description of the system

The studied system is depicted in Fig. 1. It consists of a three-phase 2-Level VSC supplied by a DC voltage source. On the AC side, the VSC is connected to an AC grid through an $L_f C_f L_c$ filter. The AC grid is represented by an ideal AC voltage source in series with its equivalent impedance (L_g, R_g).

In this paper, v_m represents the modulated voltage by the converter, i_s the output current through the filter L_f, e_g the AC voltage across the capacitor C_f, i_g the grid current through the transformer inductance L_c, v_{pcc} the AC voltage at the point of common coupling (PCC) and u_{dc} the DC voltage.

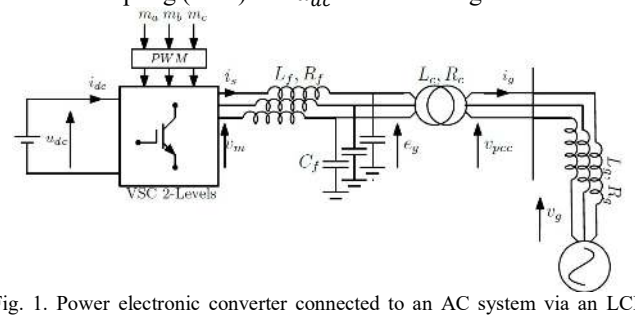

Fig. 1. Power electronic converter connected to an AC system via an LCL filter.

B. Grid-forming control structure

Fig. 2 presents the grid-forming cascaded control structure. The control consists of an inner cascaded AC voltage and current loops represented in the synchronous rotating frame (SRF) [8]. The inner control is ensured by two cascaded proportional-integral controllers (PI), feedforward decoupling terms and compensations. The AC voltage loop determines the current reference to the current control, and generates the modulated voltage to the linearization stage that delivers the modulation signals to the switching stage of the power converter. The control angle θ_{VSC} and the AC voltage references $e^*_{g_{dq}}$ are provided by a primary control based on the droop control $P-\omega$ and $Q-E_g$.

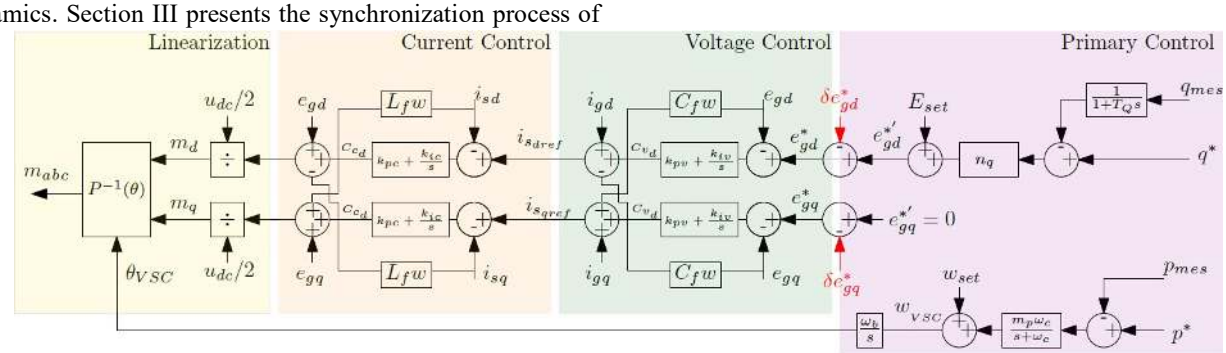

Fig. 2. Grid-forming control structure

The primary control is expressed by the following equations:

$$\omega_{VSC} - \omega_{set} = m_p \omega_b \frac{\omega_c}{\omega_c + s}(p^* - p_{mes}) \quad (1)$$

$$e_{gd}^* - E_{set} = n_q \left[\left(\frac{1}{1+T_Q s}\right) q_{mes} - q^*\right] \quad (2)$$

ω_b, ω_{set}, ω_{VSC}, m_p and n_q are respectively the nominal frequency in rad/s, the nominal grid frequency in per-unit, the internal frequency, the active and reactive droop gains. ω_c and T_Q denote the cut-off frequency and the time constant of the low-pass filters in the active and reactive droops, respectively. The low-pass filter in the reactive power droop aims only to filter the measurement, while, its role on the active power droop is usually twofold: it is used to filter the measurement and also to provide inertia to the system.

For the active power droop, the low-pass filter can be placed on the active power measurement p_{mes}, or on the error between p_{mes} and p^*. However, the second possibility gives an exact equivalence with the swing equation of the synchronous machine [24]. Moreover, it eliminates the zero of the closed loop transfer function of the active power [6].

C. Virtual impedance for current limitation

1) Recall on the virtual impedance principle

To cope with various kinds of events, a current limitation strategy has to be implemented. In this paper, the virtual impedance strategy for current limitation is adopted [12].

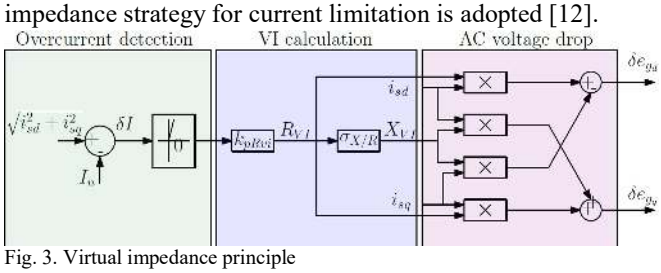

Fig. 3. Virtual impedance principle

As illustrated in Fig. 3, the VI operation principle is divided into three main phases:

- Overcurrent detection and activation (i.e.; Activation only when the current exceeds its nominal value $I_n = 1$ p.u).
- Virtual impedance calculation.
- AC voltage drop calculation.

The expressions of X_{VI}, and R_{VI} are given in (3a) and (3b).

$$X_{VI} = \begin{cases} k_{p_{R_{VI}}} \sigma_{X/R} \delta I & if\ \delta I > 0 \\ 0 & if\ \delta I \leq 0 \end{cases} \quad (3a)$$

$$R_{VI} = X_{VI}/\sigma_{X/R} \quad (3b)$$

where $\delta I = I_s - I_n$. $k_{p_{R_{VI}}}$ and $\sigma_{X/R}$ are defined respectively as the virtual impedance proportional gain and the virtual impedance ratio.

The parameter $k_{p_{R_{VI}}}$ is tuned to limit the current magnitude to a suitable level I_{max} during overcurrent in the steady state, while $\sigma_{X/R}$ ensures a good system dynamics during the overcurrent. The tuning method of these parameters is explained in [12].

When the virtual impedance is activated, the new AC voltage references are given by (4) and (5):

$$e_{gd}^* = e_{gd}^{*\prime} - \delta e_{g_d} \quad (4)$$

$$e_{gq}^* = -\delta e_{g_q} \quad (5)$$

where:

$$\delta e_{gd} = R_{VI} i_{sd} - X_{VI} i_{sq} \quad (6)$$

$$\delta e_{gq} = R_{VI} i_{sq} + X_{VI} i_{sd} \quad (7)$$

2) Impact of the virtual impedance on the system dynamics

A simplified quasi-static model including the virtual impedance is derived with the following assumptions:

- The inner control dynamics are neglected.
- The resistive effect is neglected since $X \gg R$.

The simplified model in Fig. 4 gathers actual electrical variables I_g , V_g and the AC voltage E_g modified by the virtual impedance X_{VI}. In quasi static operation, it is possible to calculate the active power with the classical formula:

$$p_{mes} = \frac{E_g{}' V_g}{X_c + X_g + X_{VI}} sin(\delta) \quad (8)$$

δ denotes the angle between the virtual VSC voltage E_g' and the grid AC voltage v_g.

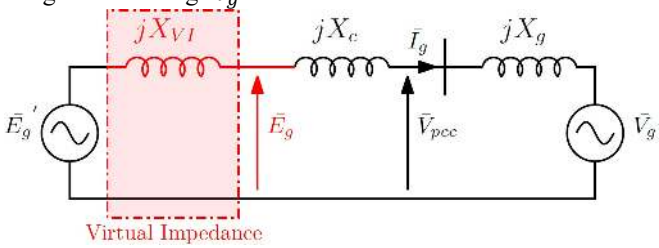

Fig. 4. Simplified quasi-static grid-forming model including VI

Assuming the angle δ is small, a second-order simplified system including the droop control is obtained as shown in Fig.5.

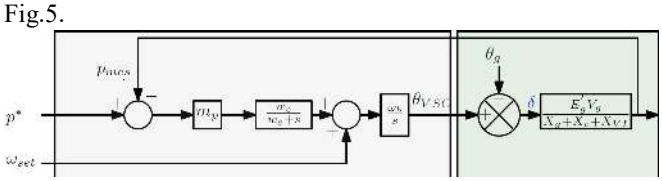

Fig. 5. Quasi-static model of the VSC based droop control

The closed loop expression of the transfer function $p*/p_{mes}$ can be expressed as follow:

$$\frac{p*}{p_{mes}} = \frac{1}{1 + \left(\frac{X_c + X_g + X_{VI}}{m_p E_g{}' V_g}\right) s + \left(\frac{X_c + X_g + X_{VI}}{m_p \omega_c E_g{}' V_g}\right) s^2} \quad (9)$$

where the damping ratio ζ and the natural frequency ω_n are:

$$\zeta = \frac{1}{2}\sqrt{\frac{(\omega_c(X_c + X_g + X_{VI}))}{m_p E_g{}' V_g}}, \quad \omega_n = \sqrt{\frac{(m_p \omega_c E_g{}' V_g)}{(X_c + X_g + X_{VI})}} \quad (10)$$

The analytical formula (10) reveals the following information:

- When X_{VI} increases, the system becomes more damped (i.e.; ζ increases) and slower (i.e.; ω_n decreases).
- When m_p decreases, the system is overdamped and slower.

These considerations will be used in the following sections.

III. Post-Fault Synchronization of a Grid-Forming Converter Based Droop Control

Once the fault is cleared, the virtual impedance is disabled progressively. The power converter should be able to resynchronize to the AC grid only using local measurements. The aim of this section is to analyze the behavior in case of a large transient and to propose a method to enhance the transient stability of the grid-forming VSC based on the droop control. For the sake of simplicity, the $L_f C_f$ filter, the inner

control dynamics, and the reactive droop control are neglected in this section. The validity of these assumptions is cheeked in the next sections through time-domain simulations.

Some general trends are drawn from the simplified quasi-static model in Fig. 4. Different phases during and after the fault are explained with an increasing complexity i.e.; without and with VI, without and with inertia effect. Since these considerations are given on a very simplified model, some time-domain simulations are presented to check the trends obtained with the quasi static model.

A. Negligible inertial effect

The inertial effect is linked with the low-pass filter placed in the active power droop. This effect can be reduced so that it becomes negligible.

Based on the simplify model in Fig. 4, Fig. 6 depicts the synchronization process of the grid-forming converter subject to a three-phase bolted fault. In this first approach, the virtual impedance is not introduced (i.e. $X_{VI} = 0$).

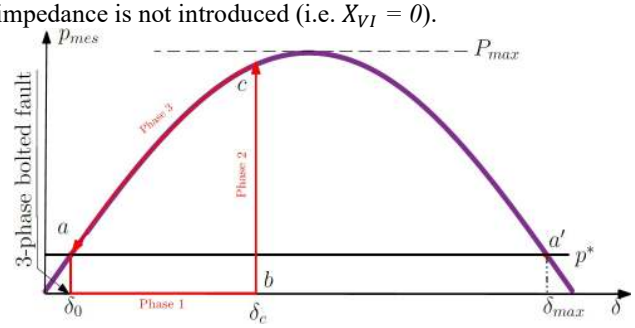

Fig. 6. $p_{mes}(\delta)$ diagram of a droop control based VSC with inertial effect

For a given p^*, there are two equilibrium points (a) and (a'), where the power p_{mes} is equal to its reference p^*. However, only the equilibrium point (a) is stable from the perspective of small-disturbance analysis [25].

The initial angle δ_0 is given by,

$$\delta_0 = asin\left(\frac{p^*}{P_{max}}\right) \tag{11}$$

where

$$P_{max} = \frac{E_g' V_g}{X_c + X_g} \tag{12}$$

The maximum angle δ_{max} of the operation point a' is expressed as,

$$\delta_{max} = \pi - \delta_0 \tag{13}$$

When a symmetrical three phase bolted fault occurs, p_{mes} drops to zero. Since the filtering effect is neglected, the frequency deviates instantaneously,

$$\omega_{VSC} = m_p p^* + \omega_{set} \tag{14}$$

Since ω_{VSC} is higher than ω_g (Hyper-synchronism), the angle increases (phase 1). When the fault is cleared, the voltage is supposed to recover instantaneously. The consequence is a straight vertical line from the operating point (b) to (c) (phase 2). During this phase $\delta = \delta_c$. δ_c denotes the clearing angle.

At the end of phase 2, p_{mes} is higher than p^* leading to $\omega_{VSC} < \omega_g$ (Hypo-synchronism). It results in a decrease of the angle from (c) to the equilibrium point (a) (phase 3). At the equilibrium point, $\omega_{VSC} = \omega_g$ and $p_{mes} = p^*$.

The stability limit is reached when the clearing angle reaches δ_{max}. This specific angle is defined as the critical clearing angle δ_{cc}. It can be concluded that when the inertial effect is neglected, $\delta_{cc} = \delta_{max}$.

B. Non-negligible inertial effect

When the inertial effect is considered, the two first phases are unchanged. However, a new phase has to be introduced as shown in Fig. 7.

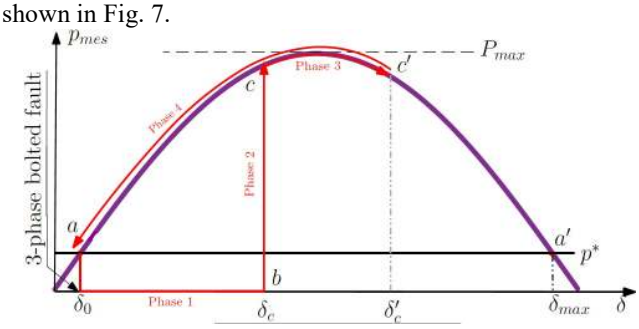

Fig. 7. $p_{mes}(\delta)$ diagram of a droop control based VSC with inertial effect

Indeed, when the fault is cleared, ω_{VSC} starts to decrease from the value calculated in (14) following the low-pass filter dynamic. As long as $\omega_{VSC} > \omega_g$, the angle keeps increasing till $\omega_{VSC} = \omega_g$ (phase 3). Once this condition is fulfilled, the angle reaches its maximum value denoted δ_c'. Then, since p_{mes} is still higher than p^*, the frequency keeps decreasing, which results in a decrease of the angle, and thereby, a movement of the operating point from (c') to the equilibrium point (a) (phase 4). Once again, at the equilibrium point, $\omega_{VSC} = \omega_g$ and $p_{mes} = p^*$.

When the inertial effect is considered, the stability limit is reached when $\delta_c' = \delta_{max}$. Hence, it can be concluded that the critical clearing angle δ_{cc} is strictly lower than δ_{max}.

C. Introduction of the virtual impedance

The effect of the virtual impedance is now introduced to embed the current limitation in this analysis. Therefore, Fig. 6 is modified when the current exceeds its rated value.

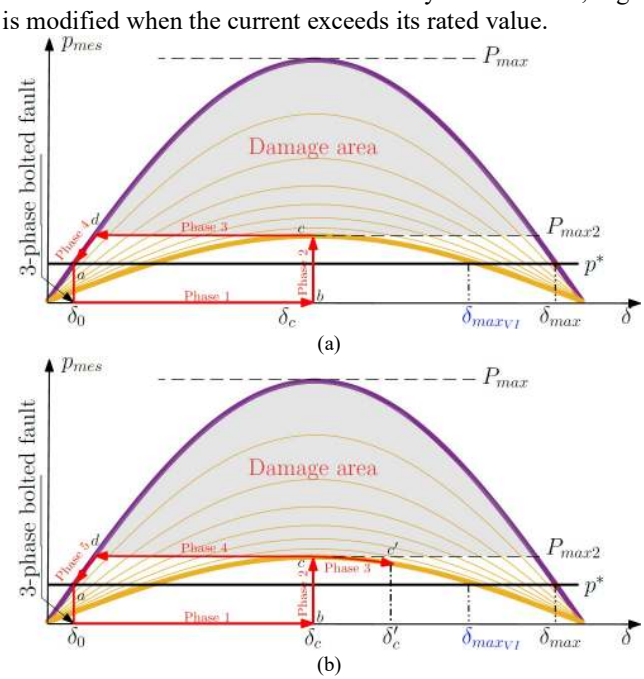

Fig. 8. $p_{mes}(\delta)$ diagram of a droop control based VSC and virtual impedance , (a) with negligible inertial effect, (b) with considerable inertial effect

The new expression of the maximum delivered active power including the virtual impedance is expressed as follow:

$$P_{max2} = \frac{E'_g V_g}{X_c + X_g + X_{VI_{max}}} \quad (15)$$

$X_{VI_{max}}$ is the virtual impedance defined from the current limit I_{max}.

Several $p_{mes}(\delta)$ may be drawn on Fig. 8.a for different values of the virtual impedance comprised between $X_{VI_{max}}$ and 0.

The sequence of operations is now modified:

- Phase 1 is similar with or without virtual impedance.
- Phase 2, the fault is cleared. As a consequence, the operating point moves first to (c), which is now located in the new curve $p_{mes} = P_{max_2} sin(\delta)$.
- Phase 3, the operating point moves from (c) to (d). In this phase, X_{VI} progressively decreases until X_{VI} is equal to zero (i.e.; when the operating point is equal to (d)).
- Phase 4, the virtual impedance is disabled and the operating point moves from (d) to the equilibrium point (a).

The activation of the virtual impedance results in a decrease of P_{max} to P_{max2} since the total impedance increases. As a consequence, the system remains stable if the fault is cleared before δ_{maxVI} expressed in (16).

$$\delta_{maxVI} = \pi - asin\left(\frac{p^*}{P_{max2}}\right) \quad (16)$$

Based on (16), a new stability limit is defined,

$$\delta_{cc} = \delta_{maxVI} \quad (17)$$

As previously explained, in case where the inertial effect is not negligible, the angle keeps diverging till (c') after the fault clearing, before recovering to the equilibrium point (a) (see Fig. 8.b). In this condition, a new stability limit is defined,

$$\delta_c{}' = \delta_{maxVI} \quad (18)$$

Then $\delta_{cc} < \delta_{max_{VI}}$.

D. Critical clearing time calculation

Thanks to the previous considerations, it is now possible to calculate the critical clearing time, which is the maximum fault duration that guarantees the stability of the system. It is determined based on the critical clearing angle. The choice has been done in this paper to calculate the critical clearing time only when the inertial effect is neglected. Indeed, it allows obtaining a simple analytical formula from which it is possible to deduce the way to enhance the transient stability.

Since p_{mes} is equal to zero during the fault, the evolution of the angle in time domain is given by the following equation,

$$\delta(t) = m_p \omega_b p^* t + \delta_0 \quad (19)$$

The critical clearing time is obtained when δ reaches δ_{cc}, which is equal to $\delta_{max_{VI}}$ as explained in the previous subsection. It yields:

$$t_c = \frac{[\delta_{\max VI} - \delta_0]}{m_p \omega_b p^*} \quad (20)$$

(20) can be also written as follow:

$$t_c = \frac{\left[\pi - asin\left(\frac{p^*}{P_{max2}}\right) - \text{asi} \quad \frac{p^*}{P_{max}}\right)\right]}{m_p \omega_b p^*} \quad (21)$$

E. Estimation of the critical clearing time from time-domain simulations

To validate the accuracy of the information found with the simplified modeling, time-domain simulations have been carried out in Matlab/SimPowerSystem with the parameters listed in Table I.

TABLE I
SYSTEM AND CONTROL PARAMETERS

Symbol	Value	Symbol	Value
P_n	1 GW	m_p	0.04 p.u.
$Cos\phi$	0.95	E_{set}	1.p.u
f_n	50 Hz	R_g	0.01 p.u.
U_{ac}	320 kV ph-ph	L_g	0.1 p.u.
$R_f = R_c$	0.005 p.u.	ω_c	62.8 rad/s
$L_f = L_c$	0.15 p.u.	n_q	0.25 p.u.
C_f	0.066 p.u.	I_n	1 p.u.
$kp_{R_{VI}}$	0.3387 p.u.	I_{max}	1.2 p.u.
k_{pc}	0.73 p.u.	k_{pv}	0.52 p.u
$\sigma_{X/R}$	10	k_{iv}	1.16 p.u.
k_{ic}	1.19 p.u.	T_Q	31.8 ms

A specific attention should be paid to the choice of ω_c (62.8 rad/s - 10 Hz). As previously mentioned, this filter has two functions:

- To filter the power measurement.
- To bring inertial effect.

Therefore, the choice of the cut-off frequency ω_c is made in such a way to keep filtering the active power measurement and to have a negligible inertial effect. This will be checked when analyzing simulation results.

Fig. 9 shows the time-domain simulation for fault duration of 154ms which corresponds to the stability limits found in simulation. This duration is close to the theoretical value of $t_c = 171ms$.

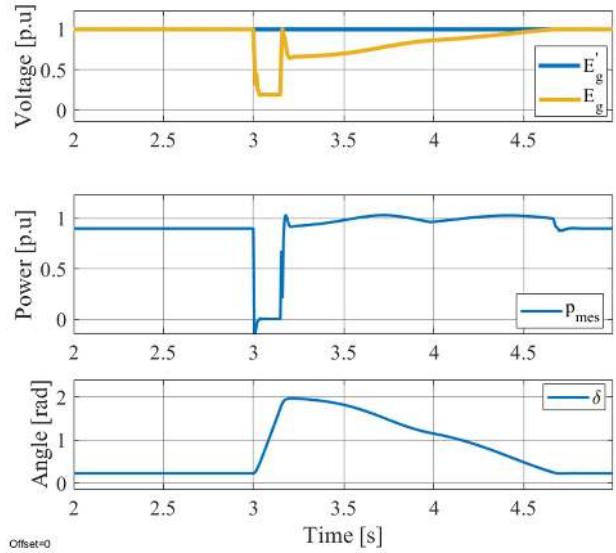

Fig. 9. Dynamic behavior of the system subjected to a three phase bolted fault.

During the fault, the active power is null as expected, the AC voltage magnitude E_g is not null due to the connection inductance X_c. Moreover, the evolution of the angle is nearly linear as found in (19). After the fault, the active power recovers following the dynamics of the droop control and the virtual impedance as shown by (10). It can be noticed that the angle starts to decrease just after the fault clearing, which confirms that the inertial effect can be neglected.

The red curve in Fig. 10 presents the dynamic $p_{mes}(\delta)$ curve. It is resulting from the time-domain simulations in Fig. 9.

Compared to the qualitative curve in Fig. 8.a, it can be noticed from the dynamic $p_{mes}(\delta)$ that the general trend of the evolution is confirmed. Indeed, the inertial effect can be neglected since the angle starts to decrease as soon as the fault is cleared.

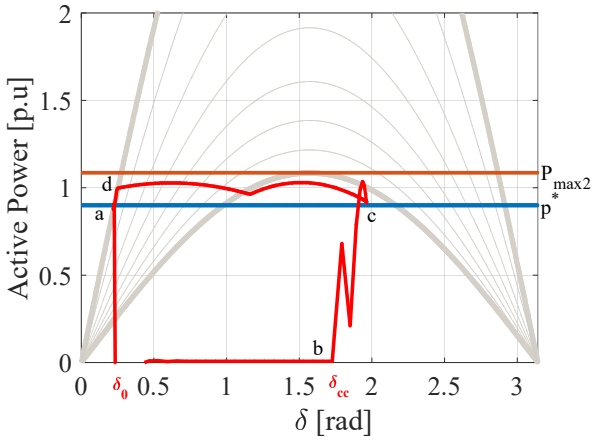

Fig. 10. Dynamic $p_{mes}(\delta)$ curves obtained from time-domain simulations with negligible inertial effect

Some differences are observed between the theoretical $p_{mes}(\delta)$ curve in Fig. 8.a and the dynamic one from Fig. 10. They can be explained by the fact that:

- The virtual impedance used for dynamic simulations takes into account the resistive effect.
- The dynamic of the grid side that prevents the AC voltage to recover instantaneously.

Additional simulation is gathered in Fig. 11 with an inertial effect of H = 5s (equivalent to $\omega_c = 2.5$ rad/s). Such a low value of the cut-off frequency leads to a poor active power damping as proved by (10). To avoid this issue, a derivative action has been added to the power loop as explained in [26].

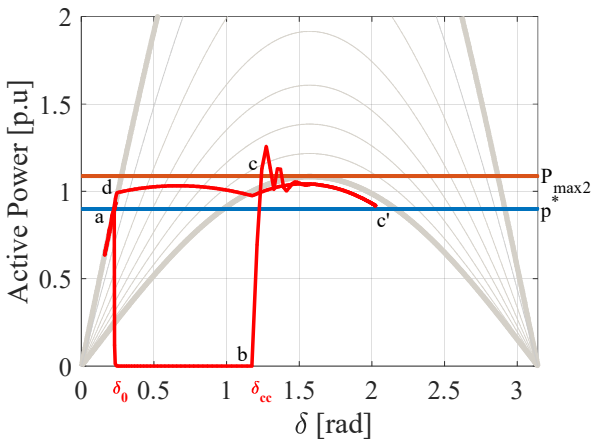

Fig. 11. Dynamic $p_{mes}(\delta)$ curves obtained from time-domain simulations with considerable inertial effect H=5s

Compared to the qualitative curve in Fig. 8.b, it can be noticed from the red dynamic $p_{mes}(\delta)$ curve drawn in Fig. 11 that the general trend of the evolution is confirmed, where the phases described previously are clearly depicted.

To have more general trends, a comparison between the critical clearing times in Fig. 12 has been achieved between three models for large range of operating points:

- The theoretical model in (21) (Yellow curve).
- The dynamic model with negligible inertia (red curve).
- The model with important inertia (H= 5s) (Blue curve).

It can be noticed that the red and yellow curves in Fig. 11 are very close. Therefore, the information drawn from the theoretical model can be considered as valid. If the inertial effect is important, the theoretical model is not valid anymore as expected. While, based on the observed results, the inertia has a positive effect on the critical clearing time as it is well-known in the conventional power system [25].

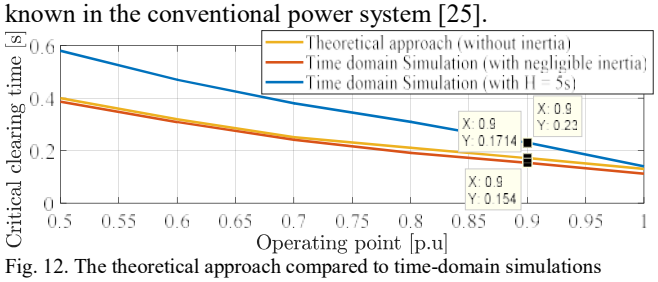

Fig. 12. The theoretical approach compared to time-domain simulations

Focusing on a system with negligible inertia, (19) and (21) highlights the large impact of the droop gain m_p on the angle evolution, and therefore, on the critical clearing time: By decreasing m_p during the fault, the critical clearing time increases and the angle evolution decreases as well, therefore, the system keeps the synchronism for a longer fault duration and recovers to its equilibrium point faster after fault clearing.

IV. Variable Droop Control for Transient Stability Enhancement

The previous section has highlighted the impact of the droop gain on the post-fault dynamics and the transient stability of the system. A question arises about the way to manage the evolution of m_p. Two different solutions are proposed in this section.

To increase the critical clearing time, m_p must be decreased. The 1st solution proposes to decrease m_p in respect to the current magnitude. The 2nd solution proposes to decease m_p in respect the AC voltage magnitude resulting from the virtual impedance.

At the end of this section, the effect of m_p is illustrated when the inertial effect is not negligible.

All the system and control dynamics neglected previously are considered in this section i.e., the $L_f C_f$ filter, the inner control dynamics, and the reactive droop control.

A. 1st solution: Adaptive droop gain in respect to the current magnitude

Intuitively, there is always a tendency to choose the current as criterion to vary the parameter mp. The aim of this section consists in showing the advantages and drawbacks of using this solution.

m_p is defined by (22). α can take two empirical values as defined in (23). If the output current exceeds its rated value, m_p is equal to one-tenth of its nominal value. Once the fault is cleared and the current returns to a safe value, the droop gain recovers to its initial value $m_p = m_{p0}$.

$$m_p = \alpha m_{p0} \tag{22}$$

$$\alpha = \begin{cases} 1, & I_s \leq 1\ \text{p.u} \\ 0.1, & I_s > 1\ \text{p.u} \end{cases} \quad (23)$$

Fig. 13 illustrates the system behavior using the 1st solution. For a given operating point $p^* = 0.9$ p.u, a 400ms fault is applied on the system. Contrary to the conventional droop control, the variable droop control ensures a stable operation even if the fault duration is much longer than the critical clearing time computed in the previous section.

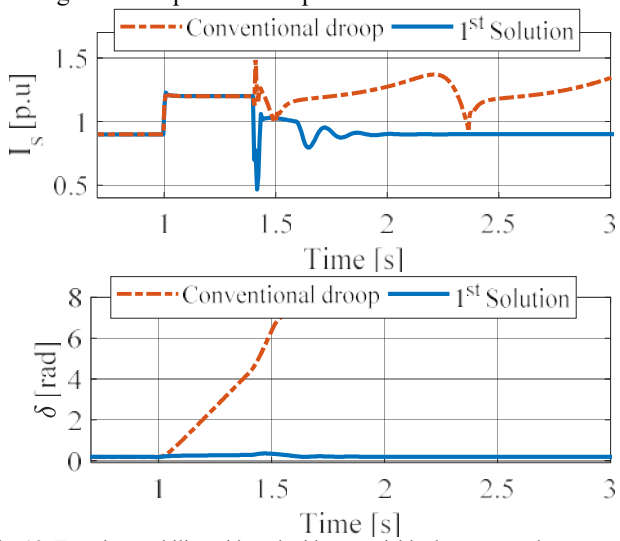

Fig. 13. Transient stability with and without variable droop control

Decreasing m_p may have a second positive side effect. In Fig. 14, the system behavior for a 75ms fault duration based on the conventional droop control ($m_p = m_{p0}$) and the variable droop control ($m_p = \alpha m_{p0}$) is analyzed. With the conventional droop control, the system needs around 800s to recover, whereas; with the variable droop control, the recovering time is around 300ms. In fact, when the droop gain decreases during the fault, the angle variation is limited as shown by (19), which explains the faster steady state recovery.

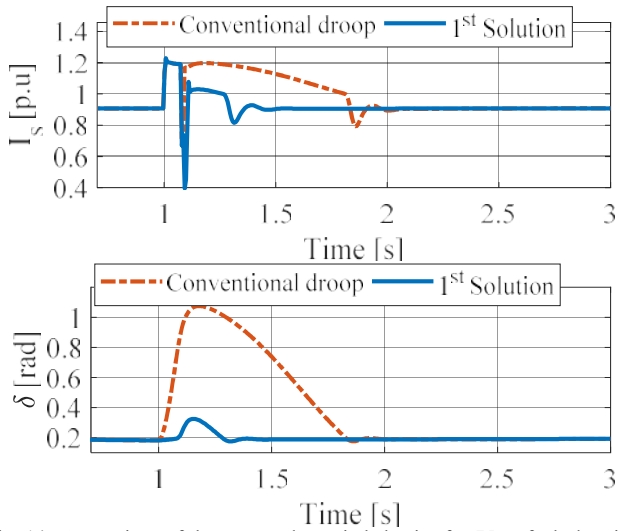

Fig. 14. Comparison of the system dynamic behavior for 75ms fault duration with constant or variable droop gain.

Nevertheless, the 1st solution may have a negative side effect if the overcurrent occurrence is due to other kinds of events. To illustrate clearly its drawback, a phase shift of 30° is performed in Fig. 15 (In power transmission systems, the phase shift are especially linked to lines tripping). When a phase shift occurs, the current increase is limited by the virtual impedance, however, the current remains higher than 1p.u, as a consequence, the droop gain m_p remains frozen in $m_p = \alpha m_{p0}$ which completely modifies the system dynamics as proved by (10), therefore, the time to resynchronize is much longer than with the conventional droop control.

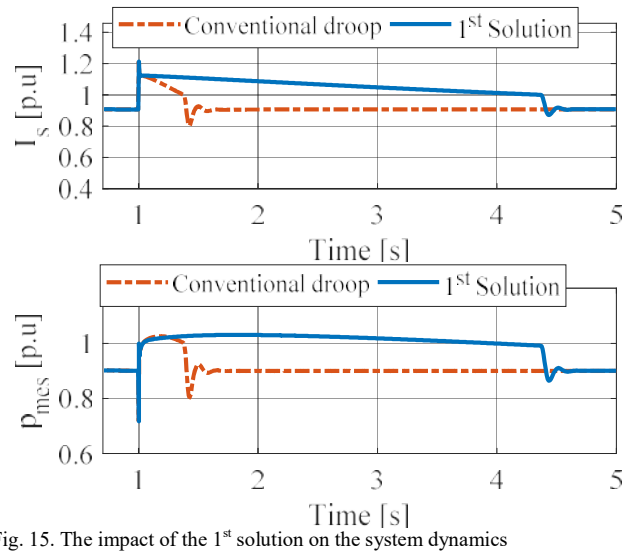

Fig. 15. The impact of the 1st solution on the system dynamics

B. 2nd Solution: Adaptive droop gain in respect with the AC voltage amplitude

The AC voltage can be considered as a good indicator of the fault nature. In case of a short circuit, the voltage is decreasing and the droop control has to be decreased either. In case of a phase shift, the voltage amplitude remains nearly the same and the droop gain does not need to be modified. A solution could be to adjust the droop value with respect to the AC voltage level. The AC voltage can be considered as a good indicator of the fault nature. In case of a short circuit, the voltage is decreasing and the droop control has to be decreased either. In case of a phase shift, the voltage amplitude remains nearly the same and the droop value does not need to be modified. A solution could be to adjust the droop value with respect to the AC voltage level. However, it may lead to unwanted noises and fast transient variations. Therefore; a proposed solution consists in using the AC voltage reference, instead of the measured one. The adaptive droop gain is expressed as follow:

$$m_p = \sqrt{e_{gd}^{*2} + e_{gq}^{*2}}\ m_{p0} \quad (24)$$

(24) shows that the droop gain can be slightly modified in case of AC voltage reference change. To avoid this effect, (25) is introduced. Hence, the droop gain is modified only when the VI is activated.

$$m_p = \sqrt{\left(1 - \delta e_{gd}\right)^2 + \delta e_{gq}^2}\ m_{p0} \quad (25)$$

During the fault, the droop gain is modified. It is possible to calculate the new droop gain in order to evaluate the new critical clearing time. During a three phase bolted fault at PCC level, the droop gain is approximately equal to $m_p = Z_c I_{max} m_{p_0} = 0.7\%$, which results in $t_c \approx 950\ ms$.

This value ensures a large stability margin compared to what is required by the present grid-code [19].

Such a small value of m_p cannot be maintained in normal operation, because it would induce a large active power variation in case of small frequency fluctuations.

The time-domain simulations of the system are performed for a 400ms fault duration (Fig. 16) and a 30° phase shift (Fig. 17). A comparison is achieved between the first and the second solution based variable droop control.

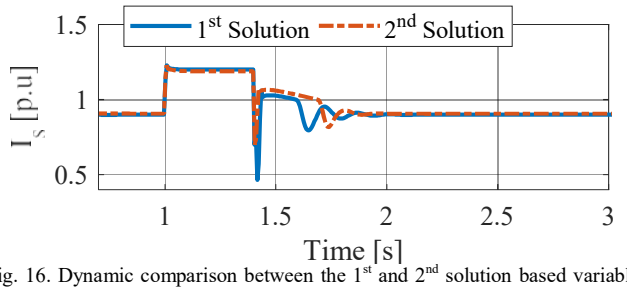

Fig. 16. Dynamic comparison between the 1st and 2nd solution based variable droop control in case of a 3-phase bolted fault.

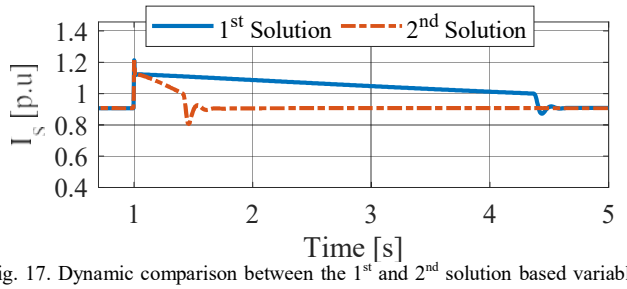

Fig. 17. Dynamic comparison between the 1st and 2nd solution based variable droop control in case 30° phase shift.

The obtained results show similar behavior in both solutions for a 3-phase bolted fault (Fig. 16). In case of a phase shift, the second solution reveals much better in terms of dynamic behavior (Fig. 17). Indeed, since the voltage is nearly constant, the droop gain is not modified so the dynamics of the system does not change too much. Therefore, it is possible to conclude that the 2nd solution is a generic solution that can cope with various overcurrent situations.

In the following simulation, the same test cases in Fig. 16 and Fig. 17 are performed, where the proposed solution is applied to the system with an inertial effect of H = 5s. Simulation results are gathered in Fig. 18 and Fig.19, respectively.

As explained in the previous section, the system based on the conventional droop control with H=5s remains stable if the fault duration is $t_c \leq 230$ ms for $p^* = 0.9$ p.u. In this context, the simulation results draw interesting results: with or without inertia effect, the proposed solution shows it effectiveness to ensure a stable operation for longer fault duration.

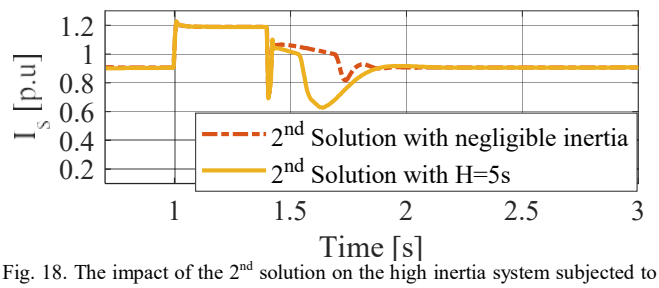

Fig. 18. The impact of the 2nd solution on the high inertia system subjected to a three phase bolted fault

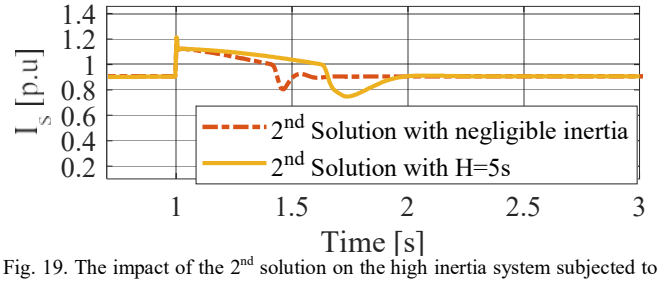

Fig. 19. The impact of the 2nd solution on the high inertia system subjected to a 30° phase shift.

V. Experimental Results

The aim of this section is to validate experimentally the theoretical developments. The experimental bench is illustrated in Fig. 20.a.

(a)

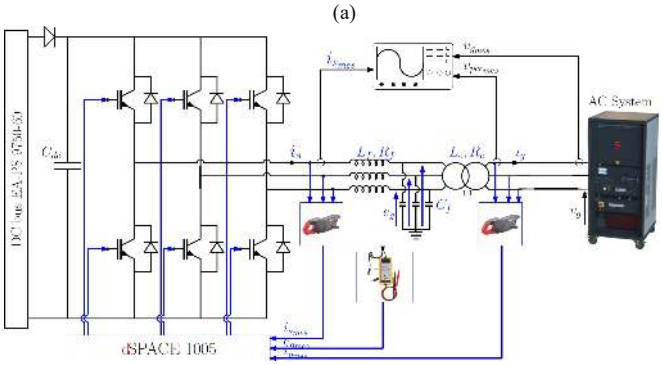

(b)

Fig. 20. The experimental bench. (a) Mockup presentation, (b) Functional schema

The 2-Level VSC (1) is supplied by an ideal and 600V DC voltage (4) source and connected to a high bandwidth AC amplifier (5) through an LCL filter (3) as presented in Fig. 20.b. The amplifier is used to emulate the AC system (i.e.; 300V ph-ph) as well as to generate the events discussed in this paper (i.e.; a 100% voltage sag emulating a 3 phase bolted fault and a phase shift). The 2-Level VSC is controlled with a dSPACE DS1005 (2) with a 40 μs time step. The switching frequency of the converter is $f_{sw} = 10kHz$.

The electrical quantities displayed in experimentation are respectively the grid voltages v_g in (abc) frame, the active power p_{mes} and the internal frequency ω_{VSC} as well as the AC voltage amplitude across the capacitor E_g and the VSC output current I_s in $d-q$ frame.

The mockup parameters are listed in Table II.

TABLE II
MOCKUP PARAMETERS

Symbol	Value
S_n	5.625 kVA
I_n	10.8A
f_n	50 Hz
L_f	10.9mH
L_c	12.9mH
C_f	9.2 μF

A. *Balanced three-phase bolted fault*

At t=t_0, $p^* = 0.7p.u$, then, a 200ms fault is applied. Fig. 21 shows the system dynamics based on the conventional droop control and Fig. 22 shows the system dynamics based on the adaptive droop control, i.e.; 2nd solution proposed in section IV.

When the fault occurred, both strategies show that the AC voltage drop induces an increase of the VSC output current I_s which is limited to 1.2 p.u thanks to the virtual impedance. The active power is not equal to zero because of the resistive part of the system. During the fault, the frequency deviation is more important with the conventional droop control resulting in a slow recovering to the equilibrium point (around 1s) as shown in Fig. 21, while, the variable droop ensures a faster post-fault synchronization (around 250ms) as shown in Fig. 22. The obtained results support the result obtained in the previous section in terms of dynamic improvement (Fig. 14).

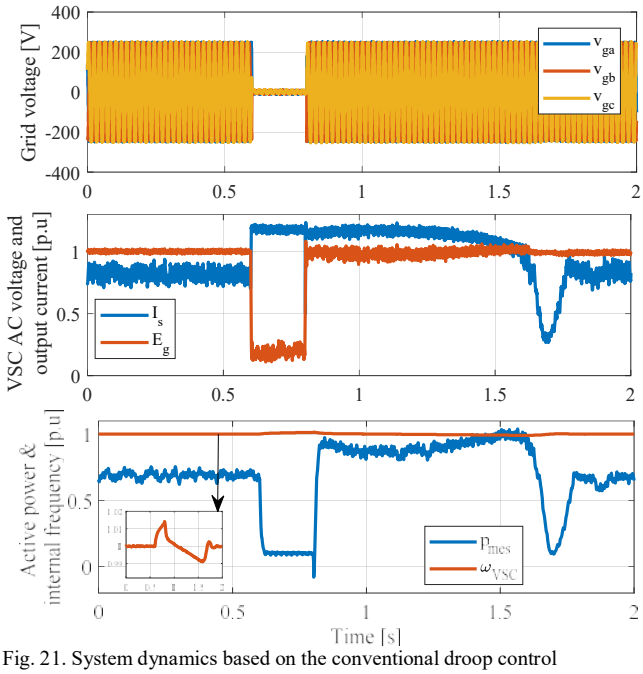

Fig. 21. System dynamics based on the conventional droop control

In the previous test cases, the fault duration was less than the critical clearing time, in Fig. 23, a 250ms fault duration is applied to the system controlled with the converntionl droop control. During the fault the current is well limited to the desired value, however, after fault clearing, the system loses the synchonization and becomes unstable. The observed unstability phenomenon is nearly similar to what has been obtained in the previous section (Fig. 13). To show the effectivness of the variable droop control, a higher fault duration has been applied to the system (400ms) as depicted in Fig. 24, once the fault is cleared, the obtained results show that the system remains stable and reaches to its equilibrium point within 300ms.

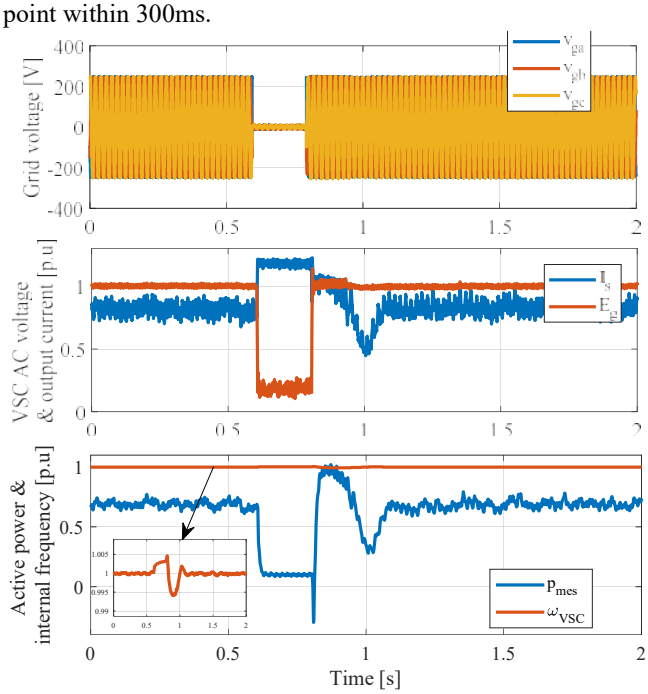

Fig. 22. System dynamics enhancement based variable droop control

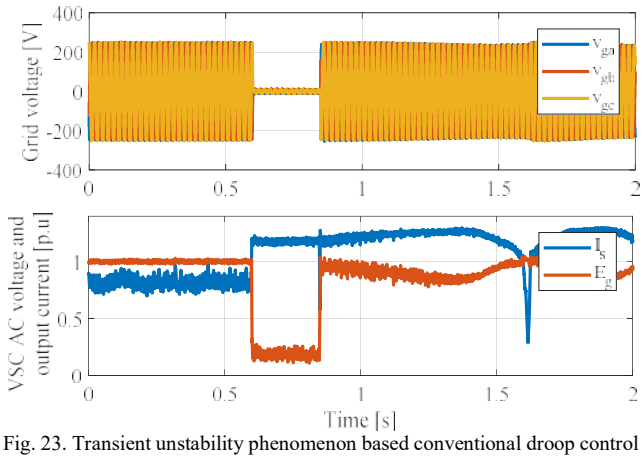

Fig. 23. Transient unstability phenomenon based conventional droop control

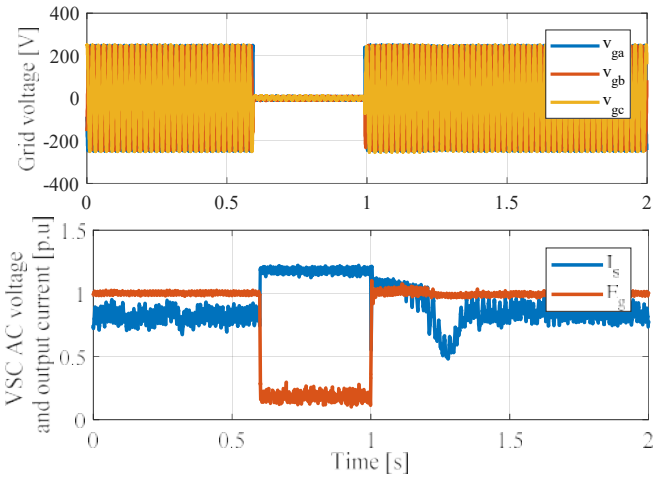

Fig. 24. Transient stability enhancement based variable droop control

B. Phase shift

In this subsection, the power reference is first set to $p^* = 0.7$ p.u and a phase-shift of 45° is then applied as illustrated in Fig. 25. The current rise to its maximum allowable value I_{max}, then, the system reaches its equilibrium point. The results obtained in Fig. 25 show the ability of the control to ensure a stable operation during a phase shift in addition to the short circuit.

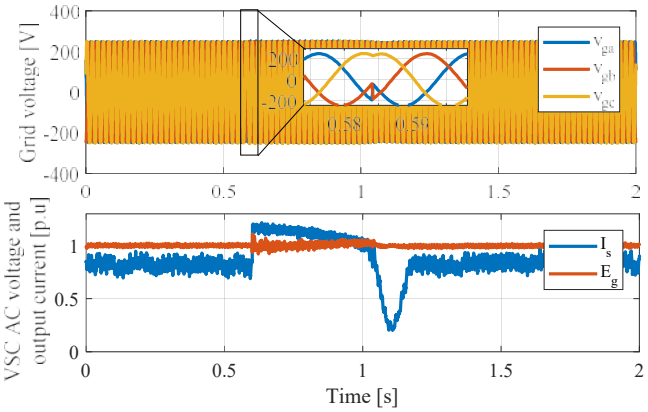

Fig. 25. Phase shift of 45°

VI. Conclusion

In this paper, the synchronization of a grid forming converter based on droop control and virtual impedance is discussed when the system is subjected to large disturbances. Neglecting the inertial effect allows to derive a simple critical clearing time analytical formula which brings out the main influent parameters on the transient stability. A method to improve the stability limit and the dynamic behavior has been proposed. Comparisons between simulation and experimentation show that the proposed simplified model is relevant for the estimation of the critical clearing time and the understanding the general behavior during the resynchronization period. Even if the inertial effect has been analyzed qualitatively, the general trends will remain effective for a droop control with inertial effect. Some future works will be devoted to more general theoretical approach including this inertial effect in the study of the transient stability of grid-forming converters. In addition, the case of asymmetrical fault will also to be considered.

References

[1] L. Zhang, L. Harnefors, and H. Nee, "Power-Synchronization Control of Grid-Connected Voltage-Source Converters," *IEEE Trans. Power Syst.*, vol. 25, no. 2, pp. 809–820, May 2010.

[2] Y. A. I. Mohamed and E. F. El-Saadany, "Adaptive Decentralized Droop Controller to Preserve Power Sharing Stability of Paralleled Inverters in Distributed Generation Microgrids," *IEEE Trans. Power Electron.*, vol. 23, no. 6, pp. 2806–2816, Nov. 2008.

[3] J. He and Y. W. Li, "An Enhanced Microgrid Load Demand Sharing Strategy," *IEEE Trans. Power Electron.*, vol. 27, no. 9, pp. 3984–3995, Sep. 2012.

[4] H. Han, Y. Liu, Y. Sun, M. Su, and J. M. Guerrero, "An Improved Droop Control Strategy for Reactive Power Sharing in Islanded Microgrid," *IEEE Trans. Power Electron.*, vol. 30, no. 6, pp. 3133–3141, Jun. 2015.

[5] Bin Li and Lin Zhou, "Power Decoupling Method Based on the Diagonal Compensating Matrix for VSG-Controlled Parallel Inverters in the Microgrid," *Energies*, vol. 10, no. 12, p. 2159, Dec. 2017.

[6] T. Qoria, Q. Cossart, C. Li, X. Guillaud, F. Gruson, and X. Kestelyn, "Deliverable 3.2: Local control and simulation tools for large transmission systems," p. 89.

[7] S. D'Arco, J. A. Suul, and O. B. Fosso, "Automatic Tuning of Cascaded Controllers for Power Converters Using Eigenvalue Parametric Sensitivities," *IEEE Trans. Ind. Appl.*, vol. 51, no. 2, pp. 1743–1753, Mar. 2015.

[8] T. Qoria, F. Gruson, F. Colas, X. Guillaud, M. Debry, and T. Prevost, "Tuning of Cascaded Controllers for Robust Grid-Forming Voltage Source Converter," in *2018 Power Systems Computation Conference (PSCC)*, 2018, pp. 1–7.

[9] B. K. Poolla, D. Groß, and F. Dörfler, "Placement and Implementation of Grid-Forming and Grid-Following Virtual Inertia and Fast Frequency Response," *IEEE Trans. Power Syst.*, pp. 1–1, 2019.

[10] G. Denis, T. Prevost, M. Debry, F. Xavier, X. Guillaud, and A. Menze, "The Migrate project: the challenges of operating a transmission grid with only inverter-based generation. A grid-forming control improvement with transient current-limiting control," *IET Renew. Power Gener.*, vol. 12, no. 5, pp. 523–529, 2018.

[11] I. Sadeghkhani, M. E. Hamedani Golshan, J. M. Guerrero, and A. Mehrizi-Sani, "A Current Limiting Strategy to Improve Fault Ride-Through of Inverter Interfaced Autonomous Microgrids," *IEEE Trans. Smart Grid*, vol. 8, no. 5, pp. 2138–2148, Sep. 2017.

[12] A. D. Paquette and D. M. Divan, "Virtual Impedance Current Limiting for Inverters in Microgrids With Synchronous Generators," *IEEE Trans. Ind. Appl.*, vol. 51, no. 2, pp. 1630–1638, Mar. 2015.

[13] G. Denis, "From grid-following to grid-forming: The new strategy to build 100 % power-electronics interfaced transmission system with enhanced transient behavior," thesis, Ecole centrale de Lille, 2017.

[14] M. Yu, W. Huang, N. Tai, X. Zheng, P. Wu, and W. Chen, "Transient stability mechanism of grid-connected inverter-interfaced distributed generators using droop control strategy," *Appl. Energy*, vol. 210, pp. 737–747, Jan. 2018.

[15] Q.-C. Zhong and G. C. Konstantopoulos, "Current-Limiting Droop Control of Grid-Connected Inverters," *IEEE Trans. Ind. Electron.*, vol. 64, no. 7, pp. 5963–5973, Jul. 2017.

[16] I. Erlich *et al.*, "New Control of Wind Turbines Ensuring Stable and Secure Operation Following Islanding of Wind Farms," *IEEE Trans. Energy Convers.*, vol. 32, no. 3, pp. 1263–1271, Sep. 2017.

[17] X. Lu, J. Wang, J. M. Guerrero, and D. Zhao, "Virtual-Impedance-Based Fault Current Limiters for Inverter Dominated AC Microgrids," *IEEE Trans. Smart Grid*, vol. 9, no. 3, pp. 1599–1612, May 2018.

[18] F. Salha, F. Colas, and X. Guillaud, "Virtual resistance principle for the overcurrent protection of PWM voltage source inverter," in *2010 IEEE PES Innovative Smart Grid Technologies Conference Europe (ISGT Europe)*, Gothenburg, Sweden, 2010, pp. 1–6.

[19] "COMMISSION REGULATION (EU) 2016/ 631 - of 14 April 2016 - establishing a network code on requirements for grid connection of generators," p. 68.

[20] K. O. Oureilidis and C. S. Demoulias, "A Fault Clearing Method in Converter-Dominated Microgrids With Conventional Protection Means," *IEEE Trans. Power Electron.*, vol. 31, no. 6, pp. 4628–4640, Jun. 2016.

[21] H. Xin, L. Huang, L. Zhang, Z. Wang, and J. Hu, "Synchronous Instability Mechanism of P-f Droop-Controlled Voltage Source Converter Caused by Current Saturation," *IEEE Trans. Power Syst.*, vol. 31, no. 6, pp. 5206–5207, Nov. 2016.

[22] L. Huang, H. Xin, Z. Wang, L. Zhang, K. Wu, and J. Hu, "Transient Stability Analysis and Control Design of Droop-Controlled Voltage Source Converters Considering Current Limitation," *IEEE Trans. Smart Grid*, vol. 10, no. 1, pp. 578–591, Jan. 2019.

[23] L. Huang, L. Zhang, H. Xin, Z. Wang, and D. Gan, "Current limiting leads to virtual power angle synchronous instability of droop-controlled converters," in *2016 IEEE Power and Energy Society General Meeting (PESGM)*, 2016, pp. 1–5.

[24] J. Liu, Y. Miura, and T. Ise, "Comparison of Dynamic Characteristics Between Virtual Synchronous Generator and Droop Control in Inverter-Based Distributed Generators," *IEEE Trans. Power Electron.*, vol. 31, no. 5, pp. 3600–3611, May 2016.

[25] Kundur, *Power System Stability And Control*. McGraw-Hill, 1994.

[26] T. Qoria, F. Gruson, F. Colas, G. Denis, T. Prevost, and X. Guillaud, "Inertia effect and load sharing capability of grid forming converters connected to a transmission grid," in *15th IET International Conference on AC and DC Power Transmission (ACDC 2019)*, 2019, pp. 1–6.